# Electronic, bonding, and optical properties of $CeO_2$ and $Ce_2O_3$ from first principles

N. V. Skorodumova,[1] R. Ahuja,[2] S. I. Simak,[1] I. A. Abrikosov,[2] B. Johansson,[2,3] and B. I. Lundqvist[1]
[1]*Department of Applied Physics, Chalmers University of Technology and Göteborg University, S-41296 Göteborg, Sweden*
[2]*Condensed Matter Theory Group, Department of Physics, Box 530, S-75121 Uppsala, Sweden*
[3]*Applied Materials Physics, Department of Materials and Engineering, Royal Institute of Technology (KTH), SE-10044 Stockholm, Sweden*

(Received 12 May 2000; revised manuscript received 2 October 2000; published 28 August 2001)

First-principles electronic structure calculations of cerium oxide in two forms, $CeO_2$ and $Ce_2O_3$, are presented. The $4f$ state of Ce is treated as a part of the inner core in $Ce_2O_3$ and as a valence-band-like state in $CeO_2$. The calculated ground-state and magnetic properties of the Ce (III) oxide are shown to be in agreement with available experimental data as well as the calculated ground-state and optical properties of Ce (IV) dioxide. The nature of the bonding in cerium oxide is discussed on the basis of an analysis of the charge-density and electron localization function distributions and described as a polarized ionic bond in both oxides.

DOI: 10.1103/PhysRevB.64.115108 PACS number(s): 71.28.+d, 71.27.+a, 71.15.Nc

## I. INTRODUCTION

Cerium oxide is a technologically important material with remarkable properties used in a number of applications. For instance, it is widely applied in automobile exhaust catalysts as an oxygen storage, due to its ability to take and release oxygen under oxidizing and reducing conditions. The cause of this effect is a continuously ongoing transformation between the two Ce oxides, the oxygen-rich $CeO_2$ and the oxygen-poor $Ce_2O_3$ depending on the external oxygen concentration.

Due to other important properties of Ce oxide, such as a high dielectric constant and good epitaxy on Si, it is also viewed as a prospective material for future microelectronic applications. In particular, $CeO_2$ is considered as a candidate for replacing silicon dioxide in electronic appliances.[1] This explains the present intensive attention drawn to this oxide and its optical properties.[2–5]

Fundamental issues and key features of the cerium oxides, like the occupation of the $4f$ orbital and bonding, are extensively discussed in the literature. They have been investigated by a number of experimental techniques, including x-ray photoemission and absorption spectroscopies and *L-M*-edge and bremsstrahlung isochromat spectroscopies, as well as optical measurements. In most cases model calculations based on the Anderson impurity model were used to analyze the experimental data.[2,6–9] As a result two opposite points of view regarding the occupation of the $4f$ orbital of Ce have been formed. One of them considers the $4f$ electron of Ce in $CeO_2$ to be in a mixed-valence state with the occupation $n_f$ of about 0.5.[6–8] To explain the coexistence of the mixed-valence features and insulating properties of $CeO_2$ the author of Refs. 6 and 7 has proposed a specific local valence-mixing mechanism between $2p$ states of O and $4f$ states of Ce. According to Ref. 7 the same mechanism exists in $\alpha$-Ce.

However, other authors, based on the results of similar experimental techniques, have come to the conclusion that the $4f$ orbital of Ce in $CeO_2$ is essentially unoccupied and the Ce ion is in the tetravalent state.[9] They show that it is not correct to consider what seems to be a partial occupation of the $4f$ Ce state as an initial state since the creation of a core hole leads to a renormalization of all the states, including the $4f$ states, and can cause the appearance of a $4f^1$ configuration.[2,9] The measurements of the optical reflectivity performed by Marabelli and Wachter have also shown that the occupation of the Ce $4f$ state is less than 5%.[2]

Consequently, the question about the nature of the bonding in $CeO_2$ is answered differently by different authors depending on their opinion regarding the occupation of the $4f$ orbital. A number of possible pictures have been put forward, such as covalent bonding[2] and ionic or partly ionic bonding,[9,10] as well as covalent bonding in the Ce-O and Ce-Ce pairs but ionic bonds between the oxygen atoms.[11] In spite of this controversy and the practical importance of the cerium oxide, to the best of our knowledge only few first-principles theoretical investigations have been carried out. In the early 1980s Koelling *et al.*[11] calculated the electronic structure of $CeO_2$ by means of the linear augmented-plane-wave (LAPW) method with Slater exchange and warped muffin-tin approximation for the crystal potential and charge density. They reported that the $f$ and $d$ states of Ce are hybridized with the oxygen $2p$ band.[12] More recently Hill and Catlow[13] applied the restricted Hartree-Fock method, well known for describing the exchange interaction correctly but entirely missing the correlation effects. They calculated the electronic and thermodynamic properties of $CeO_2$ and found that the lattice parameter is equal to 5.385 Å and the bulk modulus is equal to 357 GPa. However, the experimental value for the bulk modulus is 236 GPa (Ref. 14) (204 GPa according to Ref. 15) and, therefore, the discrepancy between the Hartree-Fock and experimental values is about 50%.

Unfortunately, little is known about the properties of $Ce_2O_3$, although it has been discussed in a few publications.[16–18] There are, for instance, results from the photoemission experiments and analysis based on the Anderson impurity model showing that Ce in $Ce_2O_3$ is close to the trivalent state.[19]

One reason for the relatively limited number of theoretical studies of Ce oxides could be the difficulty to provide a proper description of the $4f$-electron state of Ce within standard band methods as the on-site electron repulsion (''Hub-

 

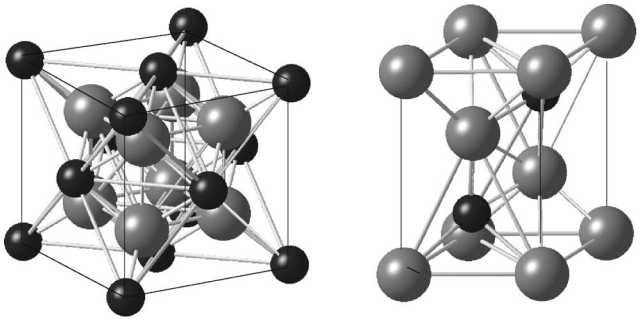


FIG. 1. Crystal structures of (a) the cubic fluorite lattice ($Fm\bar{3}m$) of $CeO_2$ and (b) the hexagonal lattice ($P\bar{3}m1$) of $Ce_2O_3$. Here Ce and O atoms are shown by black and gray circles, respectively.

bard U'') may be high compared to the bandwidth. Several methods such as LDA+U (Ref. 20) and SIC-LDA (Ref. 21) have recently been developed to deal with this type of correlated systems. In particular, they were successfully applied to describe the $\gamma$-$\alpha$ transition in pure Ce (Refs. 22–27) and properties of Ce monopnictides and chalcogenides.[28–30] In spite of this success the general applicability of these methods to systems with strong correlations still remains unclear. At the same time, a number of authors[31,32] also reported very satisfactory results for the calculated ground-state properties of $\gamma$- and $\alpha$-Ce phases, as well as for the $\gamma$-$\alpha$ transition in Ce, obtained within a much simpler band scheme, which considers one $4f$ electron in $\gamma$-Ce as fully localized by treating it as part of the inner core, whereas the $4f$ state in $\alpha$-Ce is considered as an itinerant band state.

In the present paper we extend the latter approach to the cerium oxides and present the results of *ab initio* investigations of the electronic structure, bonding, and optical properties of $CeO_2$ and $Ce_2O_3$. Stoichiometric $CeO_2$ has a cubic fluorite lattice ($Fm\bar{3}m$) with four cerium and eight oxygen atoms per unit cell[33] [Fig. 1(a)]. The sesquioxide of Ce, $Ce_2O_3$ (*A* type), has a hexagonal lattice with $P\bar{3}m1$ space group, two cerium, and three oxygen atoms per unit cell, and with a $c/a$ ratio equal to 1.55 (Ref. 33) [Fig. 1(b)]. We calculate the properties of these oxides in the framework of the full-potential linear muffin-tin orbital (FP-LMTO) method.[34] This method has been shown to be an efficient tool for calculating properties of different compounds, including oxides.[35] The description of the applied technique and details of the calculations are given in Sec. II. Section III is devoted to the obtained electronic, structural, bonding, and optical properties of $CeO_2$ and $Ce_2O_3$. A summary of the presented results is given in Sec. IV.

## II. DETAILS OF THE CALCULATION

The total energy and electronic structure have been calculated by means of the FP-LMTO method. The lattice space is divided into nonoverlapping muffin-tin spheres (MTS's) surrounding each atomic site and interstitial regions between them. No approximation for the shape of the potential and charge density is introduced. The basis of augmented linear muffin tin orbitals is employed.[36,37] Inside the MTS's the basis set, potential, and charge density are expanded in spherical harmonics, while Fourier series are used in the interstitial region. For both $CeO_2$ and $Ce_2O_3$, the spherical harmonic series expansion has been carried out up to $l=6$. The tails of the basis functions outside their parent spheres are linear combinations of Hankel and Neuman functions. As a basis set $5s$, $5p$, $5d$, $4f$, and $6s$ orbitals inside the Ce MTS's are used when the $4f$ electron is treated as a valence electron, while only $5s$, $5p$, $5d$, and $6s$ states are included in the Hamiltonian when the $f$ electron is treated as a localized core state. The basis for the O atom contains $2s$, $2p$, and $3d$ orbitals. Further, we use a so-called ''multiple basis'' where different orbitals of $l,m_l$ character connect, in a continuous and differentiable way, Hankel and Neumann functions with different kinetic energies. We perform calculations in the framework of the local-density approximation (LDA) and the generalized gradient approximation (GGA) for the exchange-correlation energy density and potential in the Perdew-Wang parametrization.[38] For sampling of the Brillouin zone (BZ) we employ the special *k*-point method[39] with a Gaussian smearing of 20 mRy taking 40 and 24 *k* points in the irreducible wedge of the Brillouin zones for $CeO_2$ and $Ce_2O_3$, respectively. We have carried out a number of tests to ensure convergence with respect to *k* points and different grids.

The investigation of optical properties is based on calculations of the dielectric function and reflectivity. The detailed description of the calculational technique in the framework of the FP-LMTO method can be found in Refs. 35 and 40. To analyze the bonding in the oxides under consideration we have calculated the density of states, band structure, charge density, and the electron localization function (ELF).[41–43]

## III. RESULTS AND DISCUSSION

### A. Electronic structure, bonding, and ground-state properties of bulk $CeO_2$

Since $CeO_2$ is experimentally known to be paramagnetic,[44] we present our results for paramagnetic $CeO_2$. As the discussion about the degree of the localization of the $4f$ Ce electron in this oxide has led to contradictory conclusions,[2,6–8] in the present study of the electronic structure and ground-state properties we have made calculations for two models. First, we treat the Ce $4f$ state as part of the valence band. Second, we consider the $4f$ electron as a fully localized core electron. The latter means that we put one electron into the $4f$ state and treat this state as a part of the inner core of the Ce. In the following discussion we will refer to these models as the valence band model (VBM) and the core state model (CSM), respectively. The ground-state properties calculated in the framework of these two models, together with available experimental and theoretical data, are summarized in Table I. One can see that the lattice parameter and the bulk modulus of $CeO_2$ obtained for the VBM are in much better agreement with experiment than those calculated for the CSM. We remark that this conclusion does not depend on the particular form of the exchange and correlation

TABLE I. Theoretical and calculated lattice parameter [$a$ (Å)] and bulk modulus [$B$ (GPa)] of $CeO_2$.

| | Valence-band model[a] | | Core-state model[a] | | HF[b] | Expt. |
|---|---|---|---|---|---|---|
| Property | LDA | GGA | LDA | GGA | | |
| $a$ (Å) | 5.39 | 5.48 | 5.56 | 5.69 | 5.385 | 5.41[c] |
| $B$ (GPa) | 214.7 | 187.7 | 144.9 | 128.8 | 357 | 236[d], 204[e] |

[a]This work.
[b]Reference 13.
[c]Reference 33.
[d]Reference 14.
[e]Reference 15.

functional; i.e., it is true for both the LDA and GGA calculations. The best agreement with the experiment is obtained within the LDA, while GGA calculations predict a bit lower bulk modulus and higher lattice parameter. Thus our study suggests that a more realistic description of Ce $4f$ states in the dioxide is given by the VBM, because within this model the Ce ion is essentially treated as being in a tetravalent state with a very small occupation of the $4f$ level. As a matter of fact, both LDA and GGA results for $CeO_2$ within the CSM are in significant disagreement with the experimental values of the ground-state parameters (Table I). The main cause for this is that with this configuration Ce is essentially treated as being in a trivalent state.

This conclusion is also supported by the details of the electronic structure of $CeO_2$ calculated in the framework of the VBM for the Ce $4f$ state which are in good agreement with the experimental data.[2,9,45] Figure 2 shows the paramagnetic density of states and band structure calculated within the LDA, where the $4f$ electron of Ce is included in the valence band. The density of states is shown in more detail in Fig. 3, where we present the partial densities of states for Ce states (upper panel) and O states (lower panel). In this figure the lowest shown band consists of $2s$ states of O and $5p$ states of Ce. The highest occupied valence band has a lot of O $2p$ character, while the narrow band situated just above the Fermi level is mainly due to $f$ states of Ce. The width of the $2p$ band is about 4 eV, and that is in good agreement with experiment[2,9,45] as well as previous calculations.[11] The energy gap between the occupied $2p$ band of O and unoccupied band of $5d$ and $6s$ states of Ce, situated above the empty $f$ band of Ce, is about 5.5 eV, which also agrees well with measurements ($\sim$6 eV).[2,9] The gap between the $2p$ O band and narrow $f$ Ce band is about 2.5 eV, which matches the 3 eV obtained in the experiment.[9] Note also that our results show the usual underestimation of the band gap within the standard density functional theory (DFT) scheme. Nevertheless, according to the calculations $CeO_2$ is a pronounced insulator.

In Fig. 3 the presence of some Ce $d$ and $f$ characters in the $p$ band of O, as well as the presence of O $2p$ states in the narrow Ce $f$ band, can be seen. This result was also obtained in the calculations by Koelling *et al.*[11] and was interpreted as a justification of the partial occupation of the Ce $f$ states.

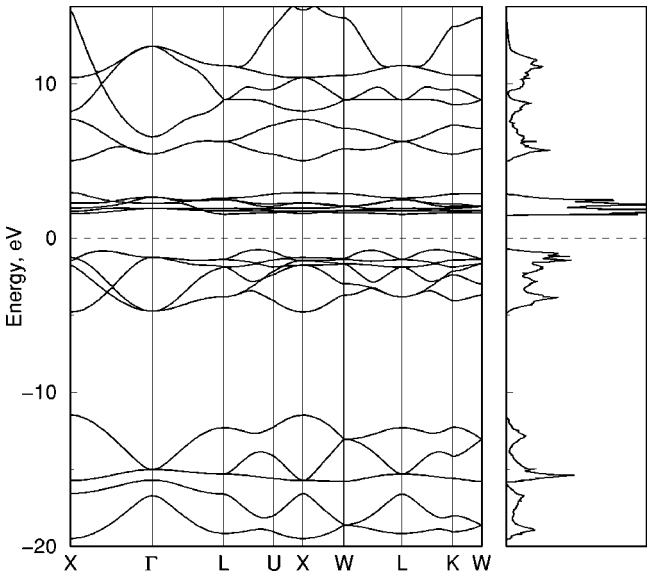


FIG. 2. Band structure (left panel) and density of states (DOS, right panel) for $CeO_2$ calculated within the valence-band model for the Ce$4f$ electron. The DOS is given in arbitrary units.

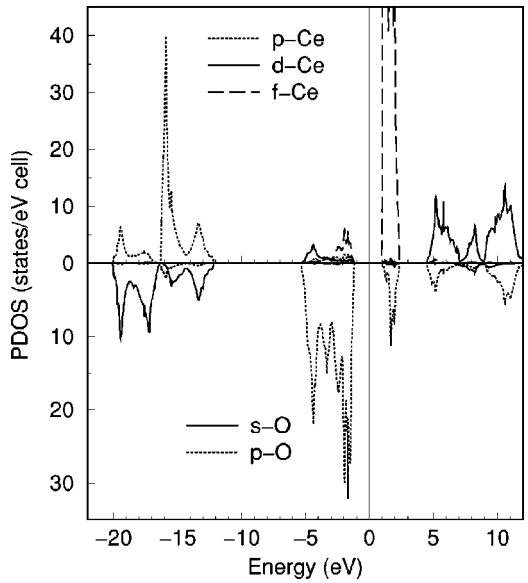


FIG. 3. Partial density of states (PDOS) for $CeO_2$ within the VBM. The upper panel shows the contribution of Ce states; the lower panel indicates O states. We have not shown the $5s$ states of Ce as they are situated quite low in energy at about $-30$ eV.

However, it is important to understand that in our calculations, as well as in the calculations reported in Ref. 11, one expands Bloch's wave functions using a basis set of atomiclike orbitals inside the MTS's which can be rather artificial. According to Andersen *et al.*[46] the role of the MTS's is to describe the input potential, rather than the output wave function. For the latter, the expansion in MT orbitals truncated outside the spheres constitutes merely a decomposition which is used in the self-consistent calculations. As a result, Ce *d* and *f* states found in the oxygen *p* band could be just tails of neighboring O electronic states spilling into the Ce MTS's. Therefore, the fact that there is a nonzero Ce *f* density of state (DOS) within the O *p* band does not necessarily mean some partial occupation of the *f* orbital or covalent bonding. As a matter of fact, the very narrow, unoccupied *f* band is situated well above the occupied valence states, which allows one to consider the $4f$ states of Ce as an empty atomiclike $4f$ level.

To support this statement we have taken a closer look at the bonding situation since the existence of real hybridization between states of Ce and O should lead to covalent bonds between these atoms. For this purpose we first analyze the charge-density distribution calculated within the VBM for this oxide. Note that the charge density is the quantity which is most accurately given by our method. The plane (110) with total charge-density distributions typical for $CeO_2$ is shown in Fig. 4(a). It is clearly seen that cerium oxide is characterized by a nearly spherical charge-density distribution around the Ce and O ions and a low charge density in the interstitial region. Compared to the charge density in the rest of the interstitial region relatively high charge-density bridges are present between the atomic spheres. A similar result was obtained in Ref. 11. In Ref. 11 the bridges were viewed as an indication of covalent bonds between Ce and O atoms due to hybridization of oxygen *p* states with partially occupied Ce *f* and *d* states. However, a judgement on the presence of covalency based on an analysis of the charge-density distribution alone should be made with care.[47] That is why the distribution of the electron-localization function (ELF) (Refs. 42–44 and 47) is also analyzed.

It has been shown that the spatial organization of ELF provides a basis for a well-defined classification of bonds.[47] The ELF is defined as $[1+(D/D_h)^2]^{-1}$, where $D$ is an excess of the local kinetic energy due to the Pauli principle. Thus $D$ is given by $\tau - t_W$, with $\tau$ being the Kohn-Sham local kinetic energy, $\tau = 1/2\Sigma|\nabla\varphi_i|^2$, where $\varphi_i$ are the Kohn-Sham orbitals, and $t_W$ is the value of $\tau$ in the absence of the Pauli principle ($\sim|\nabla\rho|^2/\rho$, $\rho$ being the charge density). $D_h$ represents $D$ for the corresponding uniform electron gas ($\sim\rho^{5/3}$). According to this definition the ELF can have values between 0 and 1, where 1 corresponds to perfect localization. In Fig. 4(b) the ELF is shown for the same plane as considered above for the charge-density distribution. The picture is quite peculiar, with almost triangular shapes of the ELF around the O atoms and a lower localization of the electrons on Ce atoms. Remarkably, although bridges between Ce and O atoms are seen in the charge-density distribution, no *shared-electron* picture between any pair of atoms, characteristic for covalent bonds,[47] is seen in the ELF. Moreover, our detailed study of the structure of the charge density shows that the main contribution to the total charge density at the Ce atoms [Fig. 4(a)] comes from the core electrons of Ce which, obviously, cannot contribute to covalency. On the other hand, the bonding has a visible polarization that is not typical for a pure ionic bonding (present in a typical ionic material, like NaCl). Thus no presence of covalency is confirmed by our ELF analysis and the bonding in cerium oxides can be characterized as polarized ionic.

### B. Optical properties of $CeO_2$

Based on the results of our electronic structure calculations, some optical properties of Ce dioxide are studied in the framework of the VBM, such as the imaginary $[\epsilon_2(E)]$ and real $[\epsilon_1(E)]$ parts of the dielectric function, as well as the reflectivity. In Fig. 5(b) the calculated $\epsilon_2(E)$ up to 25 eV is shown. For comparison the experimental data measured in this energy range are presented in Fig. 5(a). It contains the data reported by Marabelli and Wachter,[2] who have carried out reflectivity measurements between 1 meV and 12 eV at 300 K for single crystals of $CeO_2$, by Guo *et al.*,[3] who have obtained $\epsilon_2$ and $\epsilon_1$ up to 5 eV for $CeO_2$ films, and by Niwano *et al.*,[4] who have performed measurements for polycrystalline samples between 2.5 and 40 eV.

All the experimental curves show the same trend [Fig. 5(a)], namely, a sharp peak at about 3 eV and a wide peak at about 8 eV. The measurements by Niwano *et al.*[4] have also a peak at about 20 eV. The calculated $\epsilon_2$ curve also shows a sharp increase at about 2.5 eV at the first onset of the optical transitions. The second main peak is situated at about 10 eV and the third one at 21 eV. Thus the theoretical curve reveals a similar structure, reproducing the experimental behavior rather well.

The intensities obtained in the experiments and calculations are somewhat different. However, the intensities also differ between the different sets of experimental data used for the present comparison. For example, the magnitude of the first peak in our calculation is about 10. In the same units it is 5 in Refs. 2 and 7 in Ref. 3, while it is only 3 in Ref. 4. Note that in Fig. 5 we have scaled this curve with a factor of 3 to be able to show its structure better. These discrepancies could appear, for example, due to the use of different samples as well as different types of measurements in all the experiments. Another source of discrepancy could be the broadening of the experimental and theoretical curves. The degree of such broadening is seldom mentioned in experimental papers, though it can influence the intensities of the peaks. For the results presented in Fig. 5(b) Gaussian smearing with an energy width of 0.04 eV has been used. However, larger smearing widths lead to lower intensities for the heights of the peaks.

For insulators the peaks of $\epsilon_2$ originate from interband transitions from valence- into conduction-band states. According to the dipolar selection rule only transitions changing the angular momentum quantum number $l$ by unity ($\Delta l = \pm 1$) are allowed. The electronic structure of $CeO_2$ (Figs. 2 and 3) suggests that the first peak in $\epsilon_2$ at about 3 eV is due to the transition from Ce *d* to Ce *f* states, while the second

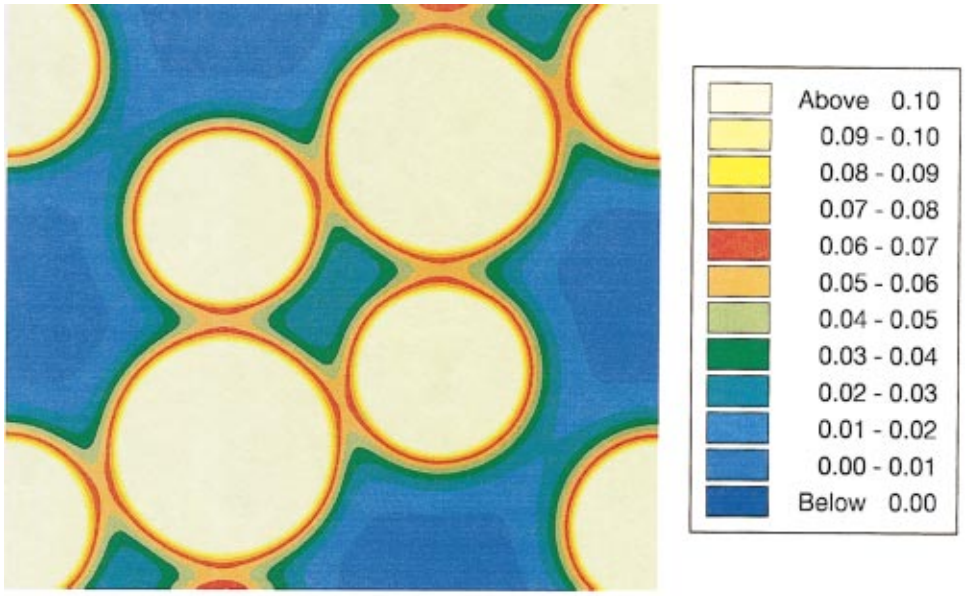


a)

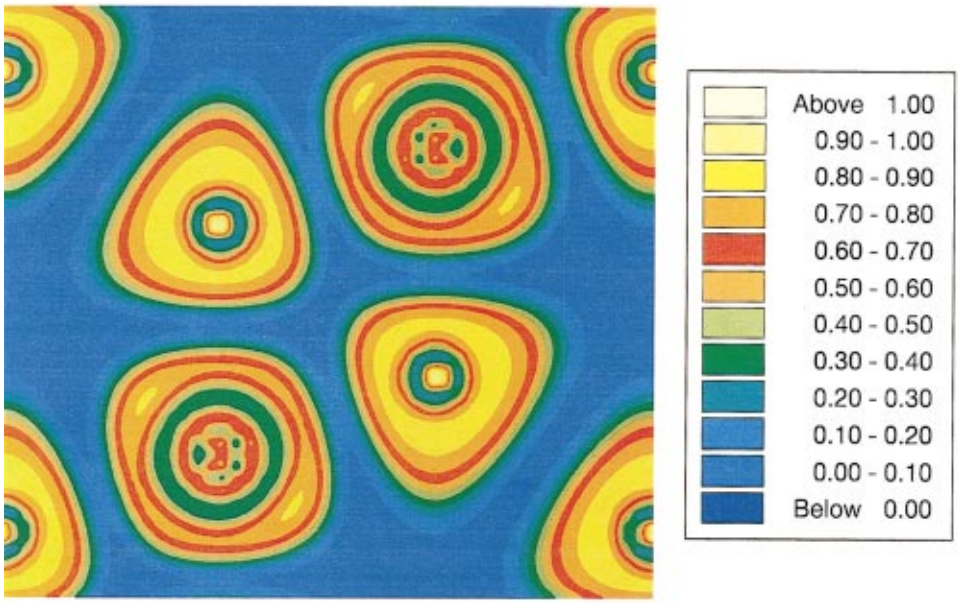


b)

FIG. 4. (Color) Total charge density (a) and electron localization function (b) for $CeO_2$.

peak corresponds to the Ce $p \rightarrow$ Ce $d$ transition. A remarkable fact regarding the first peak in $\epsilon_2$, also pointed out in Ref. 2, is that its width is essentially determined by the width of the highest occupied valence band of $CeO_2$ (about 4 eV, Fig. 2). Moreover, the fine structure of this peak in $\epsilon_2$ is similar to the fine structure of the DOS in the energy interval $-5$ to $-1$ eV. The most realistic explanation for the above observation is that the final state for the optical transitions, i.e., the unoccupied $4f$ states of Ce, is a localized atomiclike state.

The real part of the dielectric function obtained by means of a Kramers-Kronig transformation is shown in Fig. 6(b). Our results are compared to experimental data[2–4] [Fig. 6(a)] in the same way as for $\epsilon_2$. The shape of the calculated curve exhibits the same main features as the experimental results. The peak at about 2 eV corresponds to the experimental one at 3 eV, and the second quite broad peak of $\epsilon_1$ is situated at about 8 eV, corresponding to the experimental peak at 7 eV. Finally, the peak at 18 eV corresponds to the experimental peak at 21 eV.[4] Near the fundamental gap, the real part of the dielectric constant is enhanced in comparison with experiments. Our calculation gives a value of about 7 for the static dielectric constant, whereas the experimental ones are 5 (Ref.

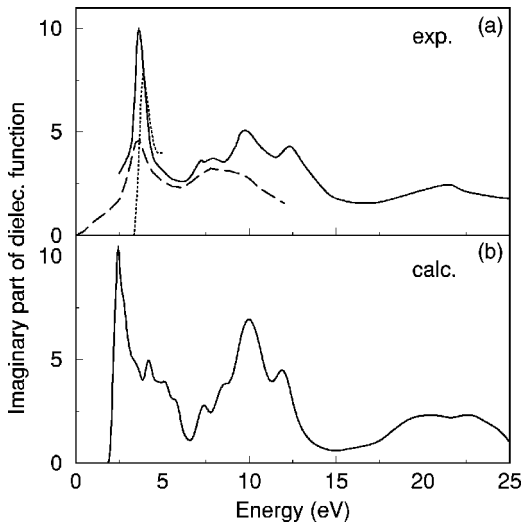


FIG. 5. Experimental (a) and calculated within the VBM (b) imaginary parts of the dielectric function for $CeO_2$. In (a) the solid, dashed, and dotted lines represent the data from Refs. 4, 2, and 3, respectively. The results from Ref. 4 have been scaled with a factor of 3.

2) or 6 (Ref. 3) and only about 3 at 2.5 eV according to Ref. 4. This type of overestimation is also observed for other materials, such as $HgI_2$.[40] The peak intensities of $\epsilon_1$ again differ for different experiments and between experiment and our calculation. The magnitude of the first peak of the calculated $\epsilon_1$ is quite comparable to the one obtained by Guo *et al.*[3] (Fig. 6).

The calculated optical reflectivity is shown in Fig. 7, together with experimental data taken from Refs. 2 and 4. The calculated reflectivity starts at about 20% and has a maximum value of roughly 35% at about 2.5 eV. The experimental reflectivity is 24% (Ref. 2) and 15% (Ref. 4) at 3.5 eV. Therefore, our result reproduces the positions of the peaks determined by interband transitions with a good accuracy (Fig. 7).

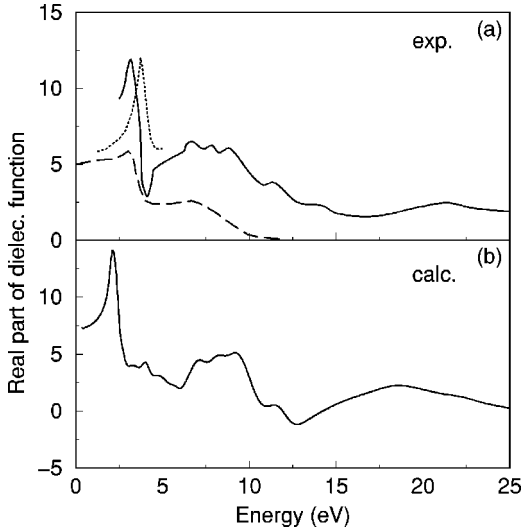


FIG. 6. Experimental (a) and calculated within the VBM (b) real parts of the dielectric function for $CeO_2$. Notations are the same as in Fig. 5.

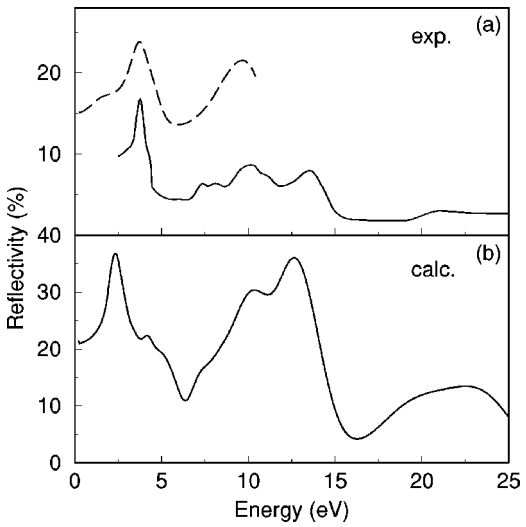


FIG. 7. Experimental (a) and calculated within the VBM (b) reflectivities for $CeO_2$. In (a) the solid and dashed lines represent data from Refs. 4 and 2, respectively.

### C. Electronic structure, bonding, and ground-state properties of bulk $Ce_2O_3$

In this section we present our results for the sesquioxide of Ce, $Ce_2O_3$ (A-type). Calculations are done for the experimental value of the $c/a$ ratio, i.e., 1.55.[33] Similarly to the case of the Ce dioxide we have considered two models for the Ce $f$ states, the VBM and the CSM for the Ce $4f$ state. The calculated structural and bonding properties and available experimental data for the oxide are presented in Table II. Unfortunately, to the best of our knowledge no experimental information regarding the bulk modulus of $Ce_2O_3$ has been reported so far. Therefore, comparison with experiment has to be limited to the lattice parameter of this oxide. One can see that considering the Ce $4f$ electron as a fully localized core state leads to results that are closest to experiments. Our GGA calculations for this model overestimate the lattice parameter value by about 2%, while the LDA calculations are essentially in agreement with experiment. On the other hand, the lattice parameter obtained for the VBM is a clear underestimate, by more than 4% for the LDA. Thus our study indicates that the description of the $4f$ electron as a localized core electron can be appropriate for this oxide.

As a matter of fact, this conclusion finds more support from a slightly deepened analysis of the calculated electronic structure of $Ce_2O_3$. In Figs. 8(a) and 8(b) we show the density of states of the oxide obtained within the CSM and the VBM, respectively. In this figure the paramagnetic density of states is shown, and the effect of magnetism will be discussed below. The treatment of the Ce $4f$ state as a delocalized band state leads to a result with a partly filled $f$ band situated right at the Fermi level [Fig. 8(b)]. However, if the $4f$ electron is kept in the core, the density of states reveals a gap between the valence and conduction bands [Fig. 8(a)], in agreement with experiment.

The highest occupied valence band of the calculated DOS corresponds to the $2p$ band of oxygen. The lowest states we

TABLE II. Theoretical and calculated lattice parameter [$a$ (Å)] and bulk modulus [$B$ (GPa)] of $Ce_2O_3$.

| | Core-state model[a] | | Valence-band model[a] | | Expt[b] |
|---|---|---|---|---|---|
| Property | LDA | GGA | LDA | GGA | |
| $a$ (Å) | 3.888 | 3.967 | 3.720 | 3.805 | 3.888 |
| $B$ (GPa) | 165.79 | 145.27 | 208.63 | 131.83 | - |

[a]This work.
[b]Reference 16.

show are composed of $5p$ states of Ce and $2s$ states of O. This structure corresponds to the x-ray photoelectron spectra of the valence band of $Ce_2O_3$ (Ref. 33) as well as to the photoemission results.[19] The energy range between the centers of the $2p$ band of O and $5p+2s$ band of Ce and O obtained in this experiment is approximately 15 eV, whereas our calculation gives 13.5 eV. The calculated gap between the valence and conduction bands is about 3 eV, which is smaller than the corresponding gap for $CeO_2$ (5.5 eV, here identified as the gap between the highest occupied valence band and the empty $d$ band of Ce), following the same tendency as the one observed in experiment.[18]

Experiments on the magnetic properties of $Ce_2O_3$ show that it is an antiferromagnet with a very low Néel temperature ($T_N$) ($\sim$9 K).[33,17] The absolute magnetic moment has been measured to be $2.17\mu_B$ per molecule[17] (the absolute moment means here a sum of the absolute values of moments on all atoms in the unit cell). Spin-polarized calculations for $Ce_2O_3$ were performed in the framework of the CSM and VBM for both ferromagnetic (FM) and antiferromagnetic (AFM) configurations. In the framework of the CSM it is assumed that each localized $4f$ electron of Ce contributes exactly $1\mu_B$ to the magnetic moment. Therefore,

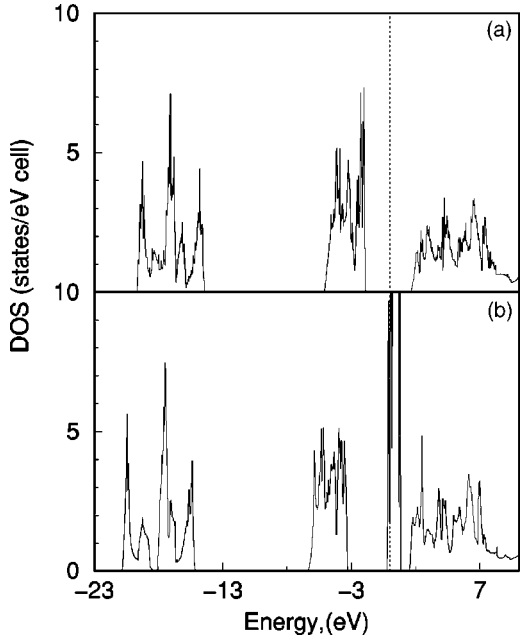


FIG. 8. Density of states (DOS) for $Ce_2O_3$ calculated within the core-state model (a) and the valence-band model (b).

since there are two Ce atoms in the unit cell, the magnetic moment of $2\mu_B$ comes from the $4f$ electrons. The rest of the magnetic moment is due to the valence $d$ band of Ce and the $p$ band of O, and it is calculated self-consistently. Within the VBM only valence electrons contribute to the magnetic moment, and it is obtained directly from our calculations.

The result of the CSM is that the AFM state is energetically more stable than the FM one, though these two configurations are nearly degenerate, the energy difference being smaller than 5 $\mu$Ry per atom. On the one hand, this is of the order of $T_N$ for this oxide. On the other hand, it is at the limit of the accuracy of our method. At the same time the calculated absolute magnetic moment is $2.13\mu_B$ for both the FM and the AFM configurations, very close to the experimental value $2.17\mu_B$.[17] Thus, the CSM accounts well for the magnetic properties of $Ce_2O_3$. On the contrary, within the VBM we have found that the FM solution for this oxide is more stable than the AFM one by 0.3 mRy per atom, and the calculated absolute magnetic moment at the equilibrium volume (situated in the vicinity of the low-spin to high-spin transition) is substantially smaller than the experimental value ($1.35\mu_B$ for the FM case and $0.72\mu_B$ for the AFM case). As a matter of fact, the magnetic moment for the high-spin solution is also quite small ($\sim 1.95\mu_B$ and $0.95\mu_B$ for the FM and AFM solutions, respectively). Therefore, the VBM leads to an unsatisfactory description of the magnetic structure of $Ce_2O_3$. Finally, we remark that the magnetic splitting of the valence band is rather small in all cases, and accordingly the paramagnetic DOS presented in Fig. 8 is quite meaningful.

Similar to the case of $CeO_2$, the bonding situation in $Ce_2O_3$ was also studied by analyzing the charge density and ELF distributions. However, for this oxide they were calculated within the CSM. In Fig. 9 the results are shown for the plane $(11\bar{2}0)$ which has an atomic arrangement similar to the (110) plane of $CeO_2$ (see Fig. 4). Thus, one can compare the charge-density and ELF distributions for these two oxides. One can see that the charge density and the ELF in $Ce_2O_3$ are essentially similar to those of $CeO_2$. The charge density is again characterized by nearly spherical distributions around the Ce and O ions and a low value in the interstitial region. The ELF has triangular shapes around the O atoms and no shared-electron picture between any pair of atoms. Thus we conclude that the bonding in $Ce_2O_3$ can be also characterized as polarized ionic.

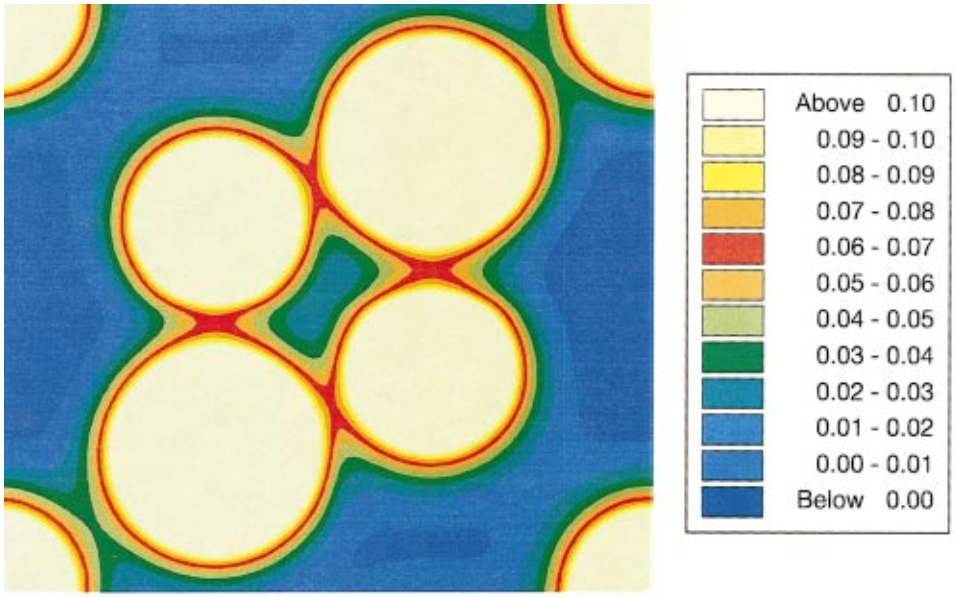


a)

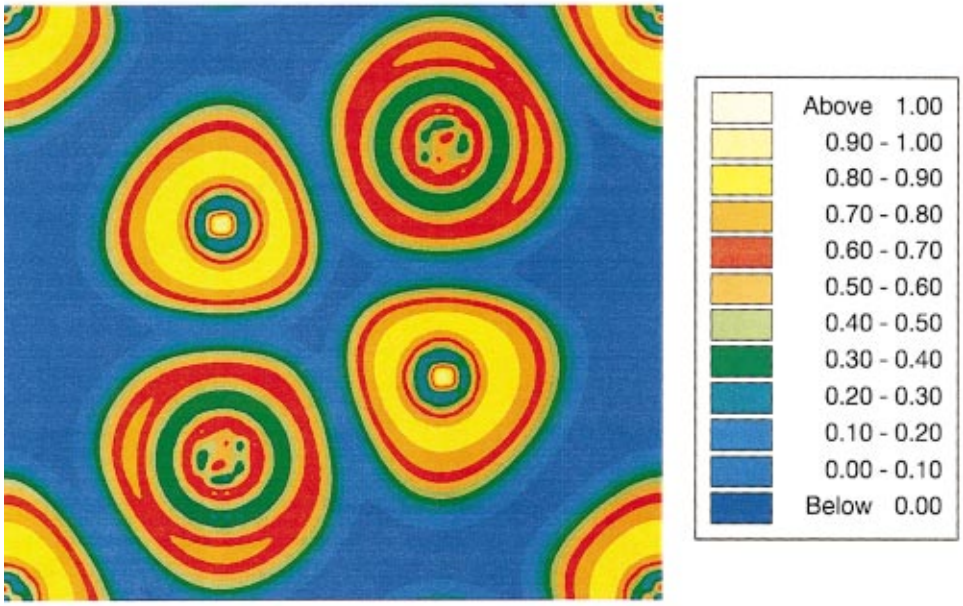


b)

FIG. 9. (Color) Total charge density (a) and electron localization function (b) for $Ce_2O_3$. (CSM)

## IV. CONCLUSIONS

We have calculated the electronic, structural, bonding, optical, and magnetic properties of the most important cerium oxides, $CeO_2$ and $Ce_2O_3$, by means of the full-potential linear muffin-tin orbital method in the framework of the density functional theory using the local density and generalized gradient approximations. The $4f$ states on the Ce atoms are treated within two simple models, as fully localized corelike states and as valence-band-like states. The former model is realized by considering the Ce $4f$ electron as a part of the inner core, while the $4f$ wave functions were included as part of the valence band in the latter model. We have obtained a better agreement with experimentally known parameters for $Ce_2O_3$ within the core-state model and within the valence-band model for $CeO_2$. Thus, we conclude that the $4f$

electron does not contribute to the bonding in $Ce_2O_3$. In the case of $CeO_2$ the calculated density of states, optical transitions, and electron localization function indicate that the unoccupied $4f$ states of Ce can be considered as essentially equivalent to an empty atomiclike $4f$ level. We have also shown that the nature of bonding in $CeO_2$ and $Ce_2O_3$ may be described as polarized ionic.

**ACKNOWLEDGMENTS**

We thank S. Dudiy for assistance with graphical applications. Support from the Swedish Research Council and the Swedish Foundation for Strategic Research (SSF) is gratefully acknowledged.

[1] T. Nakazawa, T. Inoue, M. Satoh, and Y. Yamamoto, Jpn. J. Appl. Phys., Part 1 **34**, 548 (1995).
[2] M. Marabelli and P. Wachter, Phys. Rev. B **36**, 1238 (1987).
[3] S. Guo, H. Arwin, S. N. Jacobsen, K. Järrendahl, and U. Helmersson, J. Appl. Phys. **77**, 5369 (1995).
[4] M. Niwano, S. Sato, T. Koide, T. Shidara, A. Fujimori, H. Fukutani, S. Shin, and M. Ishigame, J. Phys. Soc. Jpn. **57**, 1489 (1988).
[5] M. Veszelei, L. Kullman, C. G. Granqvist, N. Rottkay, and M. Rubin, Appl. Opt. **37**, 5993 (1998).
[6] A. Fujimori, Phys. Rev. B **27**, 3992 (1983).
[7] A. Fujimori, Phys. Rev. B **28**, 2281 (1983).
[8] F. L. Normand, J. E. Fallah, L. Hiliaire, P. Légaré, A. Kotani, and J. C. Parlebas, Solid State Commun. **71**, 885 (1989).
[9] E. Wuilloud, B. Delley, W-D. Schneider, and Y. Baer, Phys. Rev. Lett. **53**, 202 (1984).
[10] J. C. Conesa, Surf. Sci. **339**, 337 (1995).
[11] D. D. Koelling, A. M. Boring, and J. H. Wood, Solid State Commun. **47**, 227 (1983).
[12] A similar result has been lately obtained by TB-LMTO-ASA calculations: G. A. Landrum, R. Dronskowski, R. Niewa, and F. J. DiSalvo, Chem.-Eur. J. **5**, 515 (1999).
[13] S. E. Hill and C. R. A. Catlow, J. Phys. Chem. Solids **54**, 411 (1993).
[14] L. Gerward and J. S. Olsen, Powder Diffr. **8**, 127 (1993).
[15] A. Nakajima, A. Yoshihara, and M. Ishigame, Phys. Rev. B **50**, 13 297 (1994).
[16] R. W. G. Wyckoff and E. O. Wollan, Acta Crystallogr. **6**, 741 (1953).
[17] H. Pinto, M. N. Mintz, M. Melamud, and H. Shaked, Phys. Lett. **88**, 81 (1982).
[18] A. V. Golubkov, A. V. Prokofev, and A. I. Shelykh, Phys. Solid State (St. Petersburg) **37**, 1028 (1995).
[19] T. Nakano, A. Kotani, and J. C. Parlebas, J. Phys. Soc. Jpn. **56**, 2201 (1987).
[20] V. I. Anisimov, J. Zaanen, and O. K. Andersen, Phys. Rev. B **44**, 943 (1991).
[21] J. P. Perdew and A. Zunger, Phys. Rev. B **23**, 5048 (1981).
[22] Z. Szotek, W. M. Temmerman, and H. Winter, Phys. Rev. Lett. **72**, 1244 (1994).
[23] A. Svane, Phys. Rev. Lett. **72**, 1248 (1994).
[24] I. S. Sandalov, O. Hjortstam, B. Johansson, and O. Eriksson, Phys. Rev. B **51**, 13 987 (1995).
[25] A. Svane, Phys. Rev. B **53**, 4275 (1996).
[26] J. Lægsgaard and A. Svane, Phys. Rev. B **59**, 3450 (1999).
[27] D. L. Price, Phys. Rev. B **60**, 10 588 (1999).
[28] J. Lægsgaard and A. Svane, Phys. Rev. B **58**, 12 817 (1998).
[29] A. Svane, W. Temmerman, and Z. Szotek, Phys. Rev. B **59**, 7888 (1999).
[30] A. Svane, Z. Szotek, W. M. Temmerman, J. Lægsgaard, and H. Winter, J. Phys.: Condens. Matter **10**, 5309 (1998).
[31] O. Eriksson, M. S. S. Brooke, and B. Johansson, Phys. Rev. B **41**, 7311 (1990).
[32] B. Johansson, I. A. Abrikosov, M. Aldén, A. V. Ruban, and H. L. Skriver, Phys. Rev. Lett. **74**, 2335 (1995).
[33] L. Eyring, in *Handbook on the Physics and Chemistry of Rare Earths*, edited by K. A. Gschneider and L. Eyring (North-Holland, Amsterdam, 1979), Vol. 3, Chap. 27.
[34] J. M. Wills (unpublished); J. M. Wills and B. R. Cooper, Phys. Rev. B **36**, 3809 (1987); J. M. Wills, O. Eriksson, M. Alouani, and D. L. Price, in *Electronic Structure and Physical Properties of Solids*: *The uses of the LMTO method*, edited by H. Dreysse (Springer, Berlin, 2000), p. 148.
[35] B. Holm, R. Ahuja, Y. Yourdshahyan, B. Johansson, and B. I. Lundqvist, Phys. Rev. B **59**, 12 777 (1999); R. Ahuja, S. Auluck, B. Johansson, and M. A. Khan, *ibid.* **50**, 2128 (1994).
[36] O. K. Andersen, Phys. Rev. B **12**, 3060 (1975).
[37] H. L. Skriver, *The LMTO Method* (Springer-Verlag, Berlin, 1984), p. 281.
[38] J. P. Perdew and Y. Wang, Phys. Rev. B **45**, 13 244 (1992).
[39] D. J. Chadi and M. L. Cohen, Phys. Rev. B **8**, 5747 (1973); S. Froyen, Phys. Rev. B **39**, 3168 (1989).
[40] R. Ahuja, S. Auluck, O. Eriksson, J. M. Wills, and B. Johansson, Phys. Rev. B **54**, 10 419 (1996).
[41] A. D. Becke and K. E. Edgecombe, J. Chem. Phys. **92**, 5397 (1990).
[42] A. Savin, O. Jepsen, J. Flad, O. K. Andersen, H. Preuss, and H. G. Schnering, Angew. Chem. Int. Ed. Engl. **30**, 409 (1991).
[43] S. I. Simak, U. Häussermann, I. A. Abrikosov, O. Eriksson, J. M. Wills, S. Lidin, and B. Johansson, Phys. Rev. Lett. **79**, 1333 (1997).
[44] The magnetic susceptibility of $CeO_2$ has been shown to be paramagnetic; see P. Wachter, in *Valence Instabilities*, edited by P. Wachter and H. Boppart (North-Holland, Amsterdam, 1982), p. 145.
[45] Z. Hu, R. Meier, C. Schübler-Langeheine, E. Weschke, G. Kainde, I. Felner, M. Merz, N. Nücker, S. Schupper, and A. Erb, Phys. Rev. B **60**, 1460 (1999).
[46] O. K. Andersen, T. Saha-Dasgupta, R. W. Tank, C. Arcangeli, O. Jepsen, and G. Kriger, in *Electronic Structure and Physical Properties of Solids: The uses of the LMTO Method*, edited by H. Dreysse (Springer, Berlin, 2000), p. 3.
[47] B. Silvi and A. Savin, Nature (London) **371**, 683 (1994).